International Journal of Medical Microbiology 310 (2020) 151426

Contents lists available at ScienceDirect

International Journal of Medical Microbiology

journal homepage: www.elsevier.com/locate/ijmm

Myo-Inositol as a carbon substrate in *Francisella* and insights into the metabolism of *Francisella* sp. strain W12-1067

Fan Chen[a,1], Kristin Köppen[b,1], Kerstin Rydzewski[b], Rosa Einenkel[b], Clara Morguet[a], Duc Tung Vu[a], Wolfgang Eisenreich[a,**], Klaus Heuner[b,*]

[a] Department of Chemistry, Chair of Biochemistry, Technische Universität München, Garching, Germany
[b] Working Group: Cellular Interactions of Bacterial Pathogens, Centre for Biological Threats and Special Pathogens, ZBS 2, Robert Koch Institute, Berlin, Germany

ARTICLE INFO

Keywords:
Francisella sp. W12-1067
Metabolism
Glucose
Myo-inositol
Isotopolog profiling
Allofrancisella

ABSTRACT

Recently, a new environmental *Francisella* strain, *Francisella* sp. strain W12-1067, has been identified in Germany. This strain is negative for the *Francisella* pathogenicity island (FPI) but exhibits a putative alternative type VI secretion system. Some known virulence factors of *Francisella* are present, but the pathogenic capacity of this species is not known yet. *In silico* genome analysis reveals the presence of a gene cluster tentatively enabling *myo*-inositol (MI) utilization *via* a putative inositol oxygenase. Labelling experiments starting from ^{2}H-inositol demonstrate that this gene cluster is indeed involved in the metabolism of MI. We further show that, under *in vitro* conditions, supply of MI increases growth rates of strain W12-1067 in the absence of glucose and that the metabolism of MI is strongly reduced in a W12-1067 mutant lacking the MI gene cluster. The positive growth effect of MI in the absence of glucose is restored in this mutant strain by introducing the complete MI gene cluster. *F. novicida* Fx1 is also positive for the MI metabolizing gene cluster and MI again increases growth in a glucose-free medium, in contrast to *F. novicida* strain U112, which is shown to be a natural mutant of the MI metabolizing gene cluster. Labelling experiments of *Francisella* sp. strain W12-1067 in medium T containing ^{13}C-glucose, ^{13}C-serine or ^{13}C-glycerol as tracers suggest a bipartite metabolism where glucose is mainly metabolized through glycolysis, but not through the Entner-Doudoroff pathway or the pentose phosphate pathway. Carbon flux from ^{13}C-glycerol and ^{13}C-serine is less active, and label from these tracers is transferred mostly into amino acids, lactate and fatty acids. Together, the metabolism of *Francisella* sp. strain W12-1067 seems to be more related to the respective one in *F. novicida* rather than in *F. tularensis* subsp. *holarctica*.

1. Introduction

Francisella tularensis is a Gram-negative zoonotic bacterium able to cause tularemia in a wide range of animals and in humans (Ellis et al., 2002; Sjostedt, 2011). The clinically most relevant subspecies are *F. tularensis* subsp. *tularensis* (*Ftt*) exclusively found in North America and subsp. *holarctica* (*Fth*) found in the whole northern hemisphere. *F. novicida* (*Fno*) is less virulent and thought to be an opportunistic pathogen (Siddaramappa et al., 2011). *Fno* strain U112 was originally isolated from water in Utah (Larson et al., 1955). The *Fno* strain Fx1 is an isolate from a diabetic patient in Texas (Clarridge et al., 1996). In Germany, *Fth* is the only subspecies known to cause disease in patients and animals, and only one further *Francisella* species (*F.* sp. strain W12-1067 [F-W12]) has been observed so far (Faber et al., 2018; Rydzewski et al., 2014).

From a water reservoir in Germany, we identified this new *Francisella* species (Rydzewski et al., 2014) which is related to the recently published strain *F. guangzhouensis*, now renamed as *Allofrancisella* (Qu et al., 2016). However, the phylogenetic classification of new *Francisella* species may not have been completed yet (Challacombe et al., 2017; Vallesi et al., 2018). Whereas strain F-W12 is not identical to A. *guangzhouensis*, it was also isolated from a water reservoir of a cooling tower. Strain F-W12 is able to persist in a human macrophage-like cell line and in the amoeba *Acanthamoeba lenticulata,* but its virulence for mice or humans is not known yet (Rydzewski et al., 2014; Köppen et al., 2019). The draft genome of this strain was annotated and

* Corresponding author at: Cellular Interactions of Bacterial Pathogens, Centre for Biological Threats and Special Pathogens (ZBS 2), Robert Koch Institute, Seestraße 10, 13353, Berlin, Germany.
** Corresponding author at: Department of Chemistry, Chair of Biochemistry, Technische Universität München, Lichtenbergstr. 4, 85747, Garching, Germany.
E-mail addresses: wolfgang.eisenrich@ch.tum.de (W. Eisenreich), HeunerK@rki.de (K. Heuner).
[1] Both authors contributed equally to this work.

https://doi.org/10.1016/j.ijmm.2020.151426
Received 19 June 2019; Received in revised form 6 April 2020; Accepted 29 April 2020

various virulence genes common to the genus *Francisella* are present, but the *Francisella* pathogenicity island (FPI) encoding a type-VI secretion system (T6SS) is missing. However, an alternative putative T6SS (aT6SS) is present within the genome of strain F-W12 (Rydzewski et al., 2014). Using an amoebae-based scatter screen, we recently identified various fitness and putative virulence factors of this new species (Köppen et al., 2019).

The metabolic adaptation of *Francisella* is also important to efficiently replicate in host cells, as shown before for other bacteria (Eisenreich et al., 2010). Among *Francisella* species, there are differences in the usages and metabolism of diverse carbon substrates (Chen et al., 2017; Gyuranecz et al., 2010; Huber et al., 2010). Amino acids as well as glucose and glycerol can be metabolized by *Fth* and *Fno* (Chen et al., 2017; Gesbert et al., 2014, 2015; Ramond et al., 2014, 2015; Ziveri et al., 2017). Using ^{13}C-labelled substrates, it was shown that glucose is the major carbon source metabolized mainly through the Embden-Meyerhof-Parnas (EMP) pathway, and that glycerol is used as a gluconeogenetic co-substrate mainly in *Fno*, but, at lower rates, also in *Fth* (Brissac et al., 2015; Chen et al., 2017; Radlinski et al., 2018; Ziveri et al., 2017). However, genome analysis indicated that *F. tularensis* does not exhibit a phosphotransferase system or glucose-phosphate transport proteins (Meibom and Charbit, 2010). Detailed analysis of the labelling patterns in multiple metabolites suggested a bipartite metabolism in *Fth* similar to the one described earlier for *L. pneumophila* and other pathogens (Chen et al., 2017; Eisenreich et al., 2015; Gillmaier et al., 2016; Grubmüller et al., 2014).

Myo-Inositol (MI; 1,2,3,4,5,6-hexahydroxycyclohexane; $C_6H_{12}O_6$) is abundant in soil and quite common in plants and animals (Turner et al., 2002). Various different bacteria are able to grow on MI as the sole carbon source (Kröger et al., 2010; Lim et al., 2007; Yoshida et al., 2008). The phosphorylated form (inositol hexakisphosphate) is also called phytate which serves as an important carbon and phosphorus storage compound in plants and seeds. The compound can be degraded by the enzymatic activity of phytases to MI and free phosphate (Lim et al., 2007; Rao et al., 2009). Some bacteria use a MI oxygenase (glucuronate-utilizing pathway) to convert MI to glucuronic acid and in further steps to 3-phosphoglycerate (3-PG) and pyruvate (Pyr) (Ashwell et al., 1960; Kilgore and Starr, 1959; Peekhaus and Conway, 1998). Another known catabolic pathway of MI, the *iol* operon uses a MI dehydrogenase (IolG) as the first step to convert MI finally to DHAP and acetyl-CoA (Anderson and Magasanik, 1971).

In this work, we identified in the genome of F-W12 a gene cluster involved in the metabolism of MI. ^{2}H-Labelling experiments confirmed that this strain can take up and metabolize MI. On the basis of ^{13}C-labelling experiments, substrate usages and metabolic carbon fluxes through the core metabolic network of F-W12 were elucidated in considerable detail.

2. Materials and methods

2.1. Strains, media and growth conditions

Strains used in this study were *Francisella* sp. strain W12-1067 (F-W12) (Rydzewski et al., 2014); F-W12 ΔMyo mutant strain (this work) and its complemented strain (+ FIV2-Myo, this work), F-W12 Sc#50 (*glk*::Tn5, glucokinase) mutant strain (Köppen et al., 2019) and its complemented strain (*glk*::Tn5 + FIV2-*glk*, this work), *Fno* strain U112 (ATCC 15482) (Larson et al., 1955) and *Fno* strain Fx1 (Clarridge et al., 1996). *Francisella* strains were cultivated in medium T (MT) (Becker et al., 2016; Pavlovich and Mishan'kin, 1987) or on MT agar plates supplemented with hemoglobin and charcoal (MTKH plates) (Tlapak et al., 2018). For some growth experiments, modified media were used. Here, MT or Chamberlain's chemically defined medium (CDM) (Chamberlain, 1965) lacking glucose (MT-Glc; CDM-Glc) were supplemented with MI where appropriate (MT-Glc + MI; CDM-Glc + MI).

[U-$^{13}C_6$]glucose, [1,2-$^{13}C_2$]glucose, [U-$^{13}C_3$]Ser, and [U-$^{13}C_3$]glycerol were purchased from Eurisotop (Saarbrücken, Germany) and MI-C-$^{2}H_6$ (deuterium atoms connected to the carbon atoms) from Sigma-Aldrich (Taufkirchen, Germany).

2.2. Generation of a specific glucuronate metabolism gene negative strain of Francisella. sp. W12-1067 and its complementation

The F-W12 strain negative for MtlD, UxuA, KdgK, Eda, UxaC, MFS-SP and MIOX coding genes (contig_27 peg 278–284) was constructed by natural transformation of F-W12. To this end, a plasmid pUC57 peg 278-284::km was synthetically generated by *in vitro* DNA synthesis by GeneCust (Dudelang, Luxembourg) containing an insert sequence consisting of a kanamycin resistance gene enclosed by 1000 bp of F-W12 DNA sequence flanking the MltD and MIOX coding genes, respectively. The insert was amplified by PCR using M13U and M13R primer (O'Shaughnessy et al., 2003), Thermocycler TRIO-Thermoblock (Biometra, Göttingen, Germany) and the TopTaq DNA polymerase (Qiagen, Hilden, Germany). PCR amplification cycling conditions were set to activation at 94 °C for 3 min followed by 35 cycles of 94 °C for 30 s, 57 − 60 °C for 1 min/1000 bp and a final extension step of 72 °C for 10 min. PCR product was purified using Wizard® SV Gel and PCR Clean-Up System (Promega, Fitchburg, WI, USA), added to exponentially grown F-W12 bacteria and incubated at 30 °C and 5 % CO_2 for 3 days. Then, bacterial suspension was plated onto MTKH agar plates supplemented with kanamycin (12 µg/mL) and incubated at 37 °C and 5 % CO_2 until bacterial colonies arose. Individual clones were isolated and tested for deletion of the MtlD, UxuA, KdgK, Eda, UxaC, MFS-SP and MIOX coding genes by PCR using following primer combinations: (1) M_peg.278_F + M_peg.278_R for amplification of the whole insert resulting in a PCR product in the mutant strain of 3.8 kb (instead of 9.4 kb in wild-type), (2) M_peg.278_F + Km_Seq_1U, and (3) Km_Seq_F + M_peg278_R, both examining the Km resistance gene in the mutant strain leading to PCR products of 1.3 kb and 2.4 kb, respectively (Table 1). DNA sequencing was performed to confirm the PCR results of knock-out mutants. All primers used in this study are given in Table 1.

Table 1
Primers used in this study.

Primer	Sequence	Reference
Fha-1^{W12}	cttgcttcaatgactgggttttg	Tlapak et al., 2018
Fha-2**	attagcaatgagttagcttgttgct	Rydzewski et al., 2014
Fha-3*	ctgagaattaagccacttatatcagaat	Rydzewski et al., 2014
Fha-4^{W12}	atccaggaatctttgtaggagct	Tlapak et al., 2018
SacB_R_out	ctacgcagacaaacaatcaacgt	Tlapak et al., 2018
M13R	ggaaacagctatgaccatg	O'Shaughnessy et al., 2003
M13U	gtaaaacgacggccagt	O'Shaughnessy et al., 2003
Km_Seq_1U	gcatcgccttctatcgcctt	This work
Km_Seq_F	ctcttcagcaatatcacgggtag	This work
M_peg.278_F	gctgctttgcctaaaacaatgaa	This work
M_peg.278_R	aaaggctatcgacagggctataa	This work
Myo komp F	aaaattaccacagctacttttgat	This work
Myo komp R	ttgtttatatttcggtcggga	This work
peg.278_F	agtaggtttagctggctggatat	This work
peg.278_R	acttgtaatacgccttttgagct	This work
peg.279_F	agaagtacgtggtgttgcatatg	This work
peg.279_R	cgtccaatctagaacaggcataa	This work
peg.280_R	aaagtcatcgtcacctaaagctg	This work
peg.281_F	agagaccataaccttccttacgt	This work
peg.281_R	cttgagggaaaacagcttggtaa	This work
peg.282_F	ctacttatactcgtgagctggct	This work
peg.282_F2	caaatcctgagctacatcctgtg	This work
peg.282_R	cagtagggcacgagtatcatcta	This work
peg.283_F	ggctcgtgaaaccttgataaaga	This work
peg.283_F2	gctcctaatatcggggttctagt	This work
peg.284_R	tggatcactctcatcatggacat	This work
peg.284_R	tggatcactctcatcatggacat	This work
peg.284_R2	tgaactttatcaaaaccacagcct	This work
glk komp F	accttgagaacctactagttgaca	This work
glk komp R	gatctttatgagcttctatgtggc	This work

For trans-complementation, plasmids pFIV2-Myo (peg 278–284) and pFIV2-*glk* carrying the genes under the control of the *Fth* LVS GroESL promoter and F-W12 specific GroESL promoter were used (Tlapak et al., 2018). Therefore, genes were initially amplified using primer myo komp F/R and glk komp F/R, respectively, with Q5 PCR polymerase according to manufacturer's instruction (New England Biolabs, Ipswich, USA). 3′ A-overhangs were added by the TopTaq DNA polymerase (Qiagen, Hilden, Germany); resulted sequences were ligated into pGEM T easy vector (Promega, Madison, USA) and transformed into DH5α *E. coli*. DNA inserts were sequenced and screened for correct insert DNA sequence which was subsequently used to clone into the pFIV2-Val vector (NotI, NEB, Ipswich, USA). Plasmid pFIV2-Myo and pFIV2-*glk*, respectively, were transformed into *E. coli* and F-W12 mutant strains (ΔMyo; Sc#50 [*glk*::Tn5, Köppen et al., 2019]), respectively. Obtained F-W12 FIV2-complementation clones were examined for the presence of all MI metabolizing genes (MtlD, UxuA, KdgK, Eda, UxaC, MFS-SP and MIOX) and the *glk* gene, respectively, (Table 1) and for the episomal and chromosomal integrated form of the FIV2 vector (Tlapak et al., 2018).

2.3. ^{13}C-Labelling experiments

1 L of growth medium (MT) was supplemented with 2 g of [U-$^{13}C_6$] glucose (11 mM), 2 g of [1,2-$^{13}C_2$]glucose (11 mM), 0.3 g of [U-$^{13}C_3$] Ser (3 mM), or 2.5 g of [U-$^{13}C_3$]glycerol (25 mM), respectively. For more details, see Chen et al. (2017). Briefly, volumes of 250 mL of supplemented MT were inoculated with 2 − 4 mL of an overnight culture of F-W12 and incubated at 37 °C and 250 rpm. Cultures in MT were harvested after 26 h of incubation, where cultures had reached the stationary growth phase and the optical density at 600 nm (OD_{600}) amounted to approximately 1.7. Before harvesting, a culture aliquot was plated onto lysogeny broth (LB) agar (Bertani, 1951, 2004) to rule out the possibility of contamination. The bacteria were pelleted at 4700 g and 4 °C for 15 min. The supernatant was discarded and the bacterial pellet was autoclaved at 120 °C for 20 min. Then, the pellet was resuspended in 3 mL of water and lyophilized.

2.4. ^{2}H-Labelling experiments

1 L of growth medium (CDM-Glc) was supplemented with (i) 1.7 g of MI-C-$^{2}H_6$ (9.13 mM) and 3.9 g of MI (21.65 mM), or (ii) 1.7 g of MI-C-$^{2}H_6$ (9.13 mM), 1.7 g of [1,2-$^{13}C_2$]Glc (9.33 mM) and 3.9 g of MI (21.65 mM) and 3.9 g glucose (21.65 mM). For labelling experiments, bacteria were cultivated in MT overnight. On the next day, bacterial cultures were washed twice and grown in 200 ml supplemented CDM-Glc at 37 °C and 250 rpm (starting at OD_{600} of 0.3) until the stationary phase. The optical density at 600 nm (OD_{600}) was determined at regular intervals. An OD_{600} of ~0.8 to 1.0 correlated with stationary growth. Cultures in MI-supplemented CDM-Glc reached stationary growth at ~50 h. Before harvesting, a culture aliquot was plated onto LB agar to rule out the possibility of contamination. The bacteria were pelleted at 4700 g and 4 °C for 15 min. The supernatant was discarded, washed once with 200 ml cold PBS and the bacterial pellet was autoclaved at 120 °C for 20 min. Then, the pellet was resuspended in 3 mL of water and lyophilized.

2.5. Extraction and silylation of polar metabolites

In a 2 mL plastic tube, 10 mg of bacterial cells (dry weight) were mixed with 500 µL of glass beads (0.25–0.5 mm) and 1 mL of methanol p.a. The mixture was mechanically disrupted using a ribolyser system (6.5 s^{-1}, 20 s, 27 °C, three times). After the procedure, the mixture was centrifuged (10,000*g* for 20 min, 4 °C). The supernatant was collected into a 2 mL glass bottle. The solvent was removed by a gas flow of nitrogen. 50 µL of N-(tert-butyldimethylsilyl)-*N*-methyl-trifluoroacetamide containing 1 % tert-butyldimethylsilylchloride and 50 µL of water-free acetonitrile were added and incubated at 70 °C for 1 h. The reaction mixture was collected and subjected to GC–MS analysis.

2.6. Hydrolysis of proteins and silylation of amino acids

After the methanolic extraction, the residue was dried and collected into a 4 mL glass bottle. 2 mL of 6 M hydrochloric acid were added. The mixture was incubated at 105 °C for 15 h and then filtered. The hydrolysate was dried by a gas flow of nitrogen. 200 µL of 50 % acetic acid were added. After 3 min, the mixture was treated on an ultrasonic bath and then loaded onto a small column of Dowex 50 W X8 (7 × 10 mm; 200–400 mesh, 34–74 µm, H + -form). After washing with 2 mL of water, the amino acids were eluted with 1 mL of 4 M ammonia water into a 2 mL glass bottle. Under nitrogen flux, the solvent was removed. 50 µL of N-(tert-butyldimethylsilyl)-*N*-methyl-trifluoroacetamide containing 1 % tert-butyldimethylsilylchloride and 50 µL of water-free acetonitrile were added and incubated at 70 °C for 30 min. The reaction mixture was collected and subjected to GC–MS analysis. During hydrolysis, Cys and Trp were degraded and could therefore not be detected. Asn and Gln were converted into Asp and Glu, respectively, by the acidic treatment. The values reported below for Asp and Glu therefore represent the mean value for bacterial Glu/Gln and Asp/Asn, respectively.

2.7. Extraction of free fructose and silylation

In a 2 mL plastic tube, about 10 mg of bacterial sample (dry weight) were mixed with about 500 µL of glass beads (0.25–0.5 mm) and 1 mL of water. The bacterial cells were mechanically disrupted using a ribolyser system (6.5 s^{-1}, 20 s, 27 °C, three times). After the procedure, the mixture was centrifuged (10,000 *g* for 20 min, 4 °C) and the supernatant was collected into a 2 mL glass bottle. The solvent was removed by a gas flow of nitrogen. 100 µL of pyridine containing 4 mg of methoxamine hydrochloride were added and incubated at 30 °C for 90 min. The solvent was then removed by a gas flow of nitrogen. 100 µL of *N*-methyl-*N*-(trimethylsilyl)trifluoroacetamide were added, kept at 37 °C for 45 min, and then subjected to GC–MS analysis.

2.8. Hydrolysis of cell walls and silylation of amino sugars

After the water extraction, the residue was dried and collected into a 4 mL glass bottle. 2 mL of 6 M hydrochloric acid were added and the mixture was incubated at 105 °C for 15 h. The mixture was then filtered and the hydrolysate was dried under a flow of nitrogen gas. Catalytic amounts of ammonium sulfate and 100 µL of hexamethyldisilazane were added and kept at 120 °C for 3 h. The reaction mixture was collected and subjected to GC–MS analysis.

2.9. Hydrolysis of bacterial polysaccharides and derivatisation of glucose

In a 2 mL glass bottle, about 0.5 mg of bacterial cells (dry weight) were mixed with 0.5 mL of 3 M methanolic HCl. The mixture was incubated at 80 °C for 15 h. After cooling, the mixture was transferred into a 2 mL plastic tube and then centrifuged (10,000*g* for 20 min, 4 °C). The supernatant was collected into a 2 mL glass bottle and dried under a flow of nitrogen. 1 mL of acetone containing 2 % sulfuric acid was added. The mixture was incubated at room temperature for 1 h. 2 mL of saturated sodium chloride solution and 2 mL of saturated sodium carbonate solution were added to quench the reaction. The solution was extracted two times with 3 mL of ethyl acetate and collected into a 2 mL glass bottle. The ethyl acetate solvent was dried under a flow of nitrogen and the residue was treated with 200 µL of 50 % acetyl anhydride in water-free ethyl acetate at 60 °C for 15 h. The reaction mixture was dried under a flow of nitrogen and 100 µL of water-free ethyl acetate were added. The solution was collected and subjected to GC–MS analysis.

2.10. GC/MS analysis

All derivatives mentioned above were analysed by GC–MS using a quadrupol GCMS-QP 2010 Plus spectrometer (Shimadzu, Duisburg, Germany) as described earlier (Chen et al., 2017). Briefly, the GC column was a Silica capillary column (equity TM-5; 30 m by 0.25 mm, 0.25 µm film thickness; Sigma-Aldrich). For the analysis of silylated fructose and other polar metabolites, the column was developed at 100 °C for 2 min, then with a gradient up to 234 °C (3 °C min), later with a gradient up to 237 °C (1 °C min), and finally with a gradient up to 260 °C (3 °C min). At the end, the column was quickly heated to 320 °C (10 °C min) and held at this temperature for 2 min. For the analysis of silylated amino acids, the column was developed at 150 °C for 3 min, then with a gradient up to 280 °C (7 °C min) which was hold for 3 min. For the analysis of the diisopropylidene/acetate derivative of glucose, the column was developed at 150 °C for 3 min, then with a gradient up to 220 °C (10 °C min), followed with a gradient up to 280 °C (50 °C min) which was hold for 3 min. For the analysis of silylated amino sugars, the column was developed at 70 °C for 3 min, then with a gradient up to 310 °C (5 °C min) which was hold for 1 min.

All data were collected using the LabSolution software (Shimadzu). Each sample was analysed three times to afford technical replicates. The overall ^{13}C excess values (mol-%) and the relative contributions of isotopologues (%) were computed by an Excel-based in-house software package (Eylert et al., 2008) according to Lee et al. (Lee et al., 1991). Alternatively, ^{13}C excess and isotopologue compositions were calculated according to Ahmed et al. (Ahmed et al., 2014). The latter method uses an open source software package which can be downloaded using the following link: http://www.tr34.uni-wuerzburg.de/software_developments/isotopo/.

3. Results

3.1. The glucuronic acid metabolism cluster of Francisella sp. strain W12-1067 encodes a pathway for the metabolism of myo-inositol in Francisella

Since earlier results indicated that metabolism of F-W12 plays an important role for infection and persistence (Köppen et al., 2019), we took a closer look at the genome sequence and identified a gene cluster, putatively involved in the metabolism of MI (Fig. 1, genes indicated in black; and Tables 1 and 2). This cluster codes for homologous proteins of the glucuronic acid metabolism operon in *Fno* (see Tables 1 and 2) including a sugar transporter protein (peg 283), a MI oxygenase (MIOX, peg 284), a glucuronate isomerase (UxaC, peg 282), a mannonate oxidoreductase (MtlD, peg 278), a mannonate dehydratase (UxuA, peg 279), a 2-dehydro-3-deoxygluconate kinase (KdgK, peg 280) and a 2-keto-3-deoxy-6-phosphogluconate (KDPG) aldolase converting KDPG to pyruvate and glyceraldehyde-3-phosphate (Eda, peg 281) (Fig. 1**B**, Tables 1 and 2). A similar gene organization has been described in *Fno*-like 3523 (*F. hispaniensis*) and in TX07-7308, where it is called the glucuronic acid metabolism cluster (Siddaramappa et al., 2011). A similar operon is also found in *A. guangzhouensis* (Fig. 1**A**). The glucuronate metabolism operon of *Fno* Fx1, *F. philomiragia* ATCC 2515 and *F. hispaniensis* exhibits an additional putative melibiose (D-Gal-α(1→6)-D-Glc) transport protein (MelB) and a putative alpha-glucosidase (putative sucrase). In F-W12, *A. guangzhouensis* and *F. halioticida*, both of these genes are absent. Only pseudogenes are present and, in F-W12 and *F. halioticida*, an insertion element or integrase, respectively, seems to be responsible for the deletion of both genes. However, in *Fno* U112 and *Fth* LVS, the whole MI metabolism operon is absent (Fig. 1**A**) (Siddaramappa et al., 2011). Therefore, in contrast to *Fno* Fx1, *Fno* U122 seems to be a natural mutant of the MI metabolizing gene cluster.

In soil and in aquatic environments, MI can originate from phytate. We used the amino acid motif "RHGXRXP" (histidine phosphatase motif (Rao et al., 2009)) to perform a Blast search using the proteome of F-W12. We identified an ORF (peg 0427, see Table 2), encoding a putative phytase (multiple inositol polyphosphate phosphatase), exhibiting a Pfam His_Phos.2 motif (histidine-acid-phosphatase), which in general is able to degrade phytate to inositol and phosphate (Rao et al., 2009).

The obtained results suggested that F-W12 may be able to metabolize MI and probably also phytate. To further analyse the ability of F-W12 to metabolize MI, a ΔMyo mutant strain was generated (see Fig. 1**A** and materials and methods) lacking all seven genes of the MI cluster. The ΔMyo mutant strain grew as well as the wild-type strain in MT, whereas a *glk*::Tn5 mutant strain of F-W12 (Sc#50) showed reduced growth (supplemental Fig. S1). Then, we used MT lacking glucose (-Glc) to analyse the growth of different strains using MI as an additional energy substrate. Results are given in Fig. 2**A**. The F-W12 strain and the ΔMyo mutant strain showed reduced growth in MT-Glc and the addition of MI increased growth of the wild-type and the *glk*::Tn5 mutant strain, but not of the ΔMyo mutant (Fig. 2**A**), indicating that the MI gene cluster is indeed involved in the metabolism and utilization of MI. In addition, introducing of the whole MI gene cluster into the ΔMyo mutant restored the increased growth in MT (-Glc) in the presence of MI to higher levels when compared to the wild-type strain (Fig. 1**A**). In this experiment, we used the *glk*::Tn5 mutant strain (Sc#50) as a control. The growth reduction of the *glk*::Tn5 mutant strain in MT could be successfully restored by the introduction of the *glk* gene on the integration vector FIV2 (Fig. 2**A**). Results corroborate that the ΔMyo mutant strain showed nearly similar growth in MT with or without glucose, but MI was able to increase growth in MT-Glc significantly (Fig. 2**A**). In addition, we also performed the mentioned growth experiments with the species *Fno* U112 and *Fno* Fx1 (Fig. 2**B**). As expected, in the natural MI gene cluster negative *Fno* U112 strain, the presence of MI did not increase growth in MT-Glc, whereas MI significantly increased growth of *Fno* Fx1 (Fig. 2**B**).

3.2. Analysis of the MI metabolism of Francisella sp. strain W12-1067 using MI-C-$^2H_6$

As shown in Fig. 2**A**, MI supported growth of F-W12, suggesting that MI is indeed utilized by this species. To provide further evidence for MI metabolism in this strain, we performed ^2H-labelling experiments with F-W12 wild-type and its isogenic ΔMyo mutant growing in CDM medium supplemented with 9.13 mM MI-C-$^2H_6$ (*i.e.* MI carrying deuterium atoms at all six carbon positions). First, we tested growth of F-W12 and its ΔMyo mutant strain in CDM-Glc supplemented with MI (Fig. 2**C**). Growth of the ΔMyo mutant strain was not induced by MI, in contrast to the wild-type strain. Similar results were obtained with *Fno* Fx1 and the natural MI metabolizing gene cluster negative strain *Fno* U112 (Fig. 2**D**).

Due to the very high costs of MI-C-$^2H_6$, only a minimum set of experiments with labelled MI could be analysed. We performed labelling experiments with the wild-type strain and its isogenic ΔMyo mutant strain in the presence of MI-C-$^2H_6$ (see also supplemental Fig. S2). The ^2H-excess values and the fractional isotopolog distributions in sugars, protein-derived amino acids, free amino acids and free metabolites were determined by GC/MS analysis. Results are given in Fig. 3. The observed mass patterns indicated high levels of ^2H (up to 8 % molar excess) in sugars, protein-derived amino acids and free metabolites from F-W12 wild-type. Notably, the highest ^2H-excess values were detected in glucose and Phe probably reflecting their biosynthetic origins *via* the pentose phosphate pathway (PPP) and the fact that Phe is not present in CDM (in contrast to Tyr and other amino acids). In sharp contrast, only very low ^2H-values were observed in the same metabolites from the ΔMyo mutant (Fig. 3**A**). This provides firm evidence for the uptake and utilization of MI by enzymes encoded in the MI cluster described above (Fig. 1). Consequently, lack of these enzymes in the mutant resulted in the absence or in only low levels of ^2H-incorporation in the mutant strain.

Isotopologue profiling also revealed some insights into the

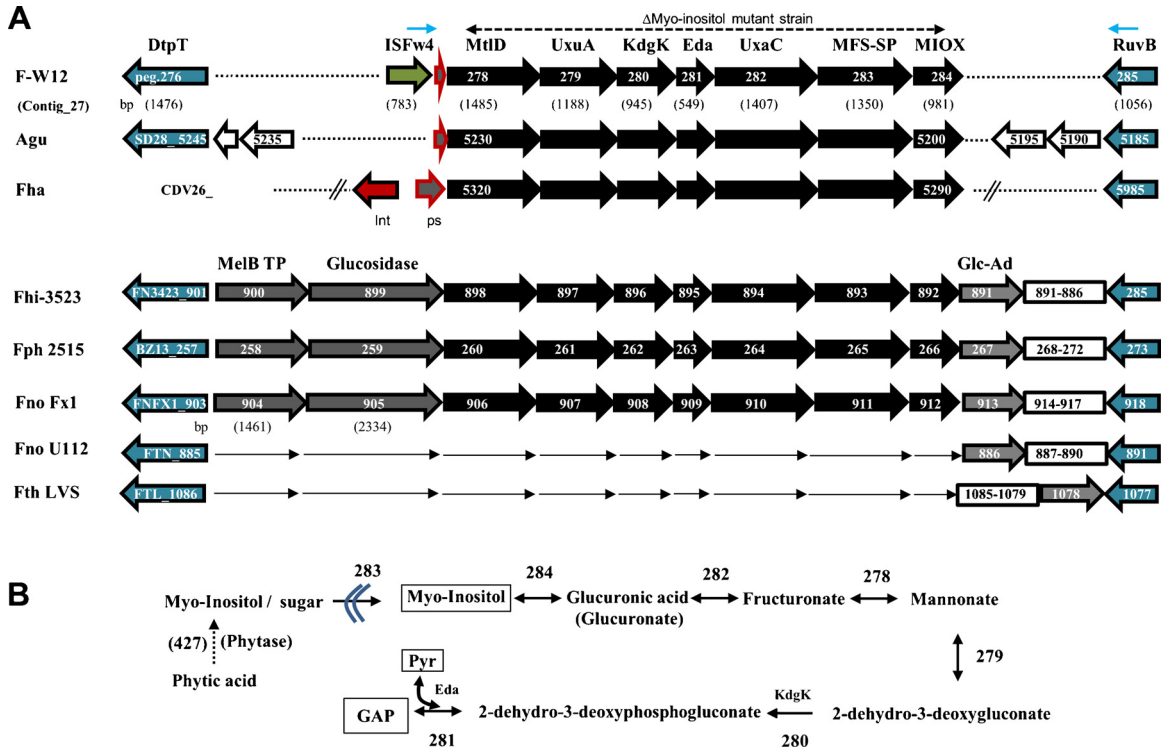

Fig. 1. The *myo*-inositol (MI) metabolizing gene cluster of *Francisella* sp. strain W12-1067. **(A)** Structure of the MI gene cluster of F-W12, *Allofrancisella guangzhouensis* (Agu), *F. halioticida* (Fha), *F. hispaniensis* 3523 (Fhi-3523), *F. philomiragia* ATCC 2515 (Fph 2515), *F. novicida* strain Fx1 (Fno Fx1), *Fno* strain U112 (Fno U112), *F. tularensis* subsp. *holarctica* strain LVS (Fth LVS). Genes are indicated by arrows, enzymes are given above and the lengths of genes are given below. Genes of the MI gene cluster are given in black. Genes deleted in the ΔMyo mutant strain of F-W12 are indicated by a double headed dotted line at the top of the figure. Light blue arrows represent primers used for the trans-complementation construct (myo komp F and myo komp R). Genes not present in a strain are indicated by thin arrows. **(B)** For catabolism, MI is taken up through a sugar transport protein (peg 283) and genes/enzymes for further degradation are shown (see also Table 2). Yet it has not been shown, if the putative phytase (peg 427) of F-W12 is involved in the degradation of phytic acid to MI. MelB TP, glucuronic (Gal-Glc alpha 1-6) transporter; glucosidase (alpha-glucosidase, putative sucrase); Glc-Ad, glucosaminidase; DtpT, Dipeptide and tripeptide permease; ISFw4, IS element number 4 of F-W12; MtlD, mannonate oxidoreductase (UxuB); UxuA, mannonate dehydratase; KdgK, 2-keto-3-deoxygluconate kinase; Eda, KDPG aldolase; UxaC, glucuronate isomerase; MFS-SP, sugar transporter; MIOX, *myo*-inositol oxygenase; RuvB, holliday junction DNA helicase; Int, integrase; ps, pseudo-gene. GAP, glyceraldehyde-3-P. (For interpretation of the references to colour in this figure legend, the reader is referred to the web version of this article).

mechanisms of MI usage. Glucose acquired one or two ^{2}H-atoms from the $^{2}H_{6}$-labelled MI tracer at relative amounts of 40 and 50 %, respectively (Fig. 3**B**). This pattern suggests that $^{2}H_{6}$-MI is converted into M + 3 isotopologs (*i.e.* carrying three ^{2}H-labels) of 2-dehydro-3-deoxy-D-gluconate serving as the precursor for the M + 1 isotopologs in pyruvate or M + 2 isotopologs of glyceraldehyde-3-P, respectively, after cleavage by the Eda enzyme (Fig. 1**B**, supplemental Fig. S2). Protein-derived Ala was characterized by M + 1 and M + 2 isotopologs at relative abundances of 80 % and 20 %, respectively. This ratio could indicate a higher flux rate to convert the M + 1 labelled pyruvate precursor into Ala in comparison to the M + 2 labelled glyceraldehyde-3-P. Phe and Tyr were mainly M + 1 and M + 2 labelled, which nicely reflects their origin from labelled pyruvate and erythrose-4-P from the PPP (Fig. 3**B**). Free amino acids resembled nearly the same isotopolog composition again indicating their origin from M + 1 isotopologs of pyruvate. Because of the downstream metabolism of M + 1 pyruvate and M + 2 glyceraldehyde-3-P *via* the citrate cycle, succinate was mainly M + 1 (43 %) and M + 2 (57 %) labelled. Dehydrogenation of M + 2 succinate then leads to the loss of one deuterium atom in fumarate now displaying over 95 % M + 1 isotopologs. Lactate displayed M + 1 and M + 2 isotopologs of 38 % and 60 %, respectively (Fig. 3**B**). Together, these results provided solid evidence that MI can be used as a carbon source by F-W12. For a better understanding of the general metabolism, we now analysed in considerable detail the main metabolic carbon pathways of this new species and of its ΔMyo mutant strain.

Table 2
Francisella sp. strain W12-1067 genes involved in MI (glucuronate) metabolism.

Peg No.*	GenBank	Protein size (aa)	Annotation/Function		FN3523 (% Id.)
278	FRA_27c02840	494	D-Mannonate oxidoreductase (UxuB)	EC 1.1.1.57	73
279	FRA_27c02850	395	Mannonate dehydratase (UxuA)	EC 4.2.1.8	86
280	FRA_27c02860	314	2-Keto-3-deoxygluconate kinase (KdgK)	EC 2.7.1.45	69
281	FRA_27c02870	182	KDPG aldolase (KdgA or Eda)	EC 4.1.3.16	65
282	FRA_27c02880	468	Glucuronate isomerase (UxaC)	EC 5.3.1.12	83
283	FRA_27c02890	449	Sugar transporter, Pfam_MFS_1	–	83
284	FRA_27c02900	326	Inositol oxygenase	EC 1.13.99.1	86
427**	FRA_31c04330	401	Phytase, putative (Pfam_HisPhos_2, signal peptide)	–	87
487	FRA_31c04980	243	Inositol-1-monophosphatase	EC 3.1.3.25	81

* From Rydzewski et al. (2014); ** function in *myo*-inositol metabolism has not been shown yet (aa), amino acids; (% Id), % identity at amino acid level.

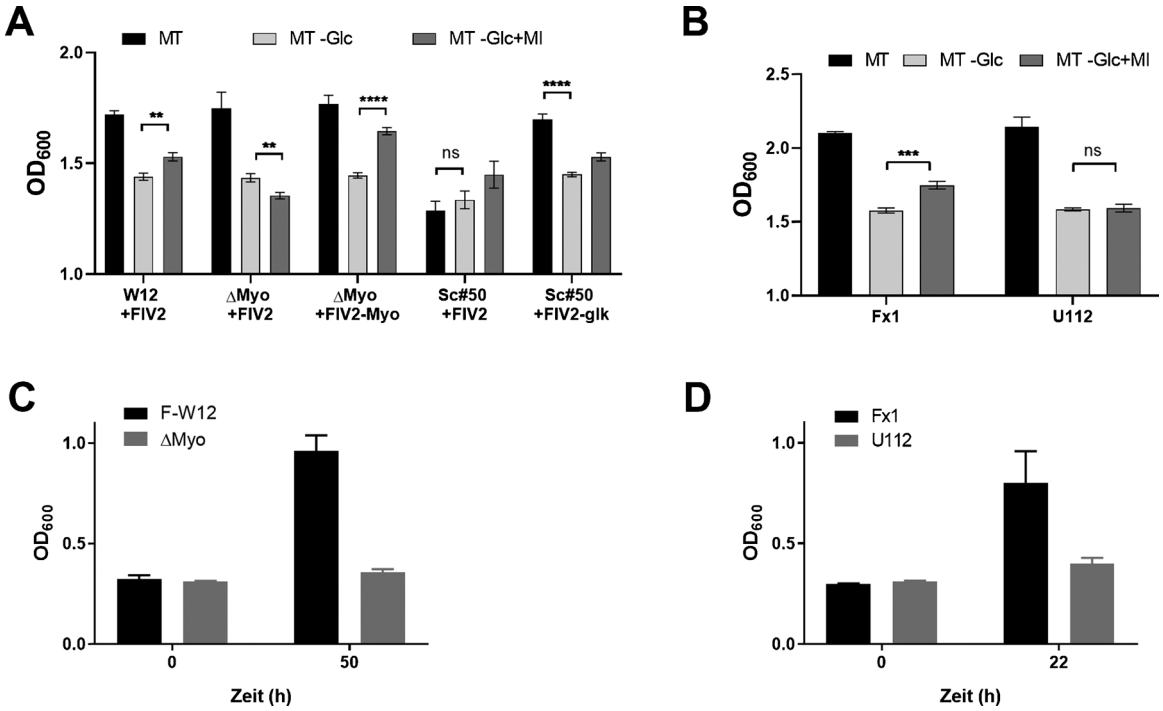

Fig. 2. Analysis of growth of *Francisella* sp. strain W12-1067 (W12 + FIV2), the isogenic ΔMyo mutant strain (ΔMyo + FIV2), the complemented ΔMyo mutant strain (ΔMyo + FIV2-Myo), the *glk*::Tn5 strain (Sc#50 + FIV2), the complemented *glk*::Tn5 strain (Sc#50 + FIV2-glk) of F-W12, the *Fno* strain Fx1 (Fx1) and the *Fno* strain U112 (U112) in different media. **(A** and **B)** Growth of respective strains in MT, in MT without glucose (MT-Glc) or in MT-Glc supplemented with MI (MT-Glc + MI) after 9 h of growth at 37 °C. A growth curve of strains in MT is given in supplemental Fig. S1. Results are means and standard deviations of three independent experiments. For statistical analysis student-*t*-tests were performed with Graphpad Prism 8 software (** $p < .01$; *** $p < .001$; **** $p < .0001$; ns, not significant). **(C)** Growth of F-W12 wild-type and ΔMyo mutant strain in CDM without glucose supplemented with 30.9 mM MI after 50 h of growth at 37 °C. Results are means and standard deviations of two independent experiments. **(D)** Growth of *Fno* strain Fx1 and *Fno* strain U112 in CDM without glucose supplemented with 111 mM MI after 22 h of growth at 37 °C. Results are means and standard deviations of two independent experiments.

3.3. Multiple substrate usage of Francisella sp. strain W12-1067 grown in medium T

Previously, we analysed the main metabolic pathways in *Fno* and *Fth*, where the bacteria were cultivated in MT in the presence of either [U-$^{13}C_6$]glucose, [U-$^{13}C_3$]glycerol, or [U-$^{13}C_3$]serine (Chen et al., 2017). On the basis of the specific ^{13}C-patterns in downstream metabolic products such as amino acids or carbohydrates, the relative incorporation rates could be determined for each labelled substrate. Moreover, the labelling distributions also shed light onto the specific

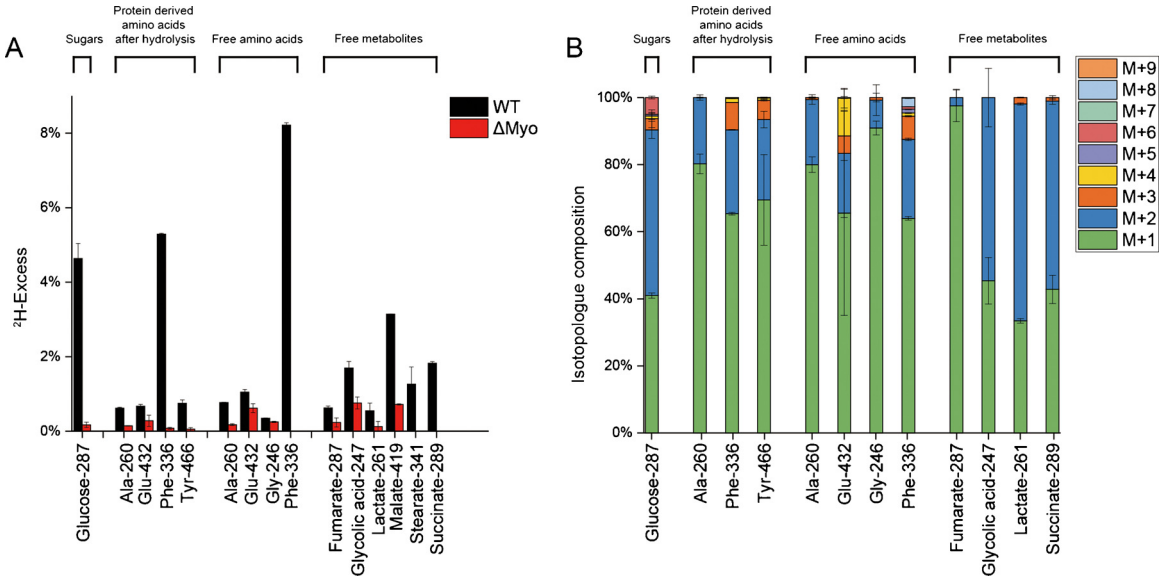

Fig. 3. (A) ^{2}H-Excess (mol%) and **(B)** the fractional isotopolog distributions (%) in key metabolites of F-W12 wild-type strain (WT) and its isogenic ΔMyo mutant (ΔMyo) grown in CDM medium supplied with 9.13 mM MI-C-$^2H_6$. ^{2}H-Excess (mol%) and relative fractions of isotopologs (%) were determined by GC/MS of silylated derivatives at the indexed *m/z* values. Error bars indicate standard deviations from the means of the 3 × technical replicates values. M + 1, M + 2, M + 3, *etc.* indicate isotopologs carrying 1, 2, 3, *etc.* ^{2}H-atoms.

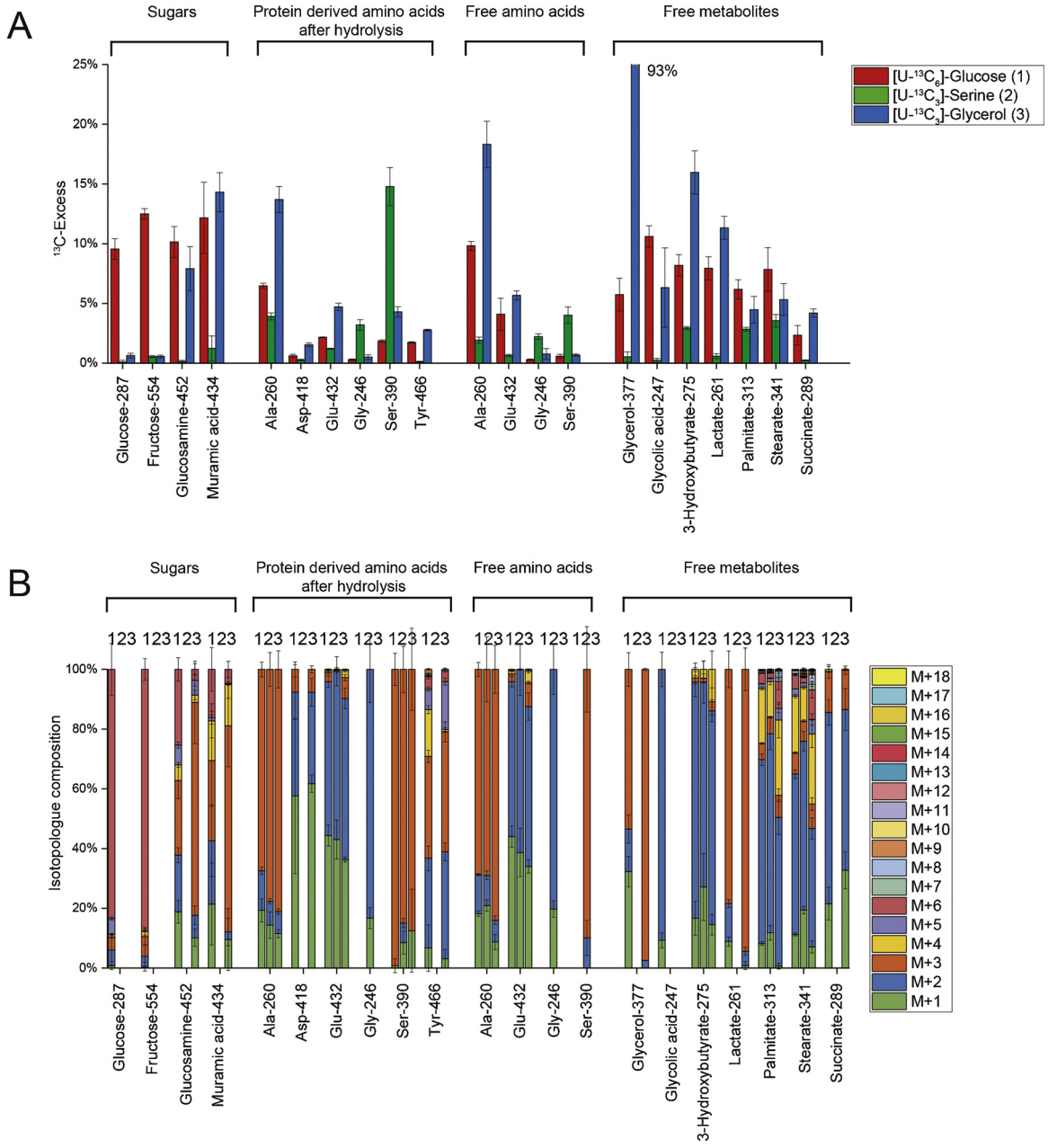

Fig. 4. (A) ^{13}C-Excess (mol%) and **(B)** the fractional isotopolog distributions (%) in key metabolites of F-W12 grown in MT supplied with 11 mM [U-$^{13}C_6$]glucose (red labels, (1)), 3 mM [U-$^{13}C_3$]serine (green labels, (2)), or 25 mM [U-$^{13}C_3$]glycerol (blue labels, (3)). ^{13}C-Excess (mol%) and relative fractions of isotopologs (%) were determined by GC/MS of the derivatives of different metabolites at the indexed *m/z* values. Error bars indicate standard deviations from the means of 6 to 9 values using 2–3 × biological replicates and 3 × technical replicates. M + 1, M + 2, M + 3, *etc.* indicate isotopologs carrying 1, 2, 3, *etc.* ^{13}C-atoms. (For interpretation of the references to colour in this figure legend, the reader is referred to the web version of this article).

pathways and fluxes starting from the supplied ^{13}C-tracers. The same experimental setting was now used for a detailed analysis of the carbon pathways in F-W12. An overview about general putative metabolic pathways of F-W12 is given in supplemental Fig. S3.

3.4. Labelling experiments with [U-$^{13}C_6$]glucose

Glucose from glycogen and cell wall-derived glucosamine/muramic acid were isolated from hydrolysates of the dried cell pellets, free fructose was extracted using water. All sugars showed ^{13}C-excess at about 10 mol% (Fig. 4**A**). As described for *Fno*, these high ^{13}C-enrichments reflected the efficient uptake of glucose also in F-W12. The main isotopolog in glycogen-derived glucose and free fructose was the M + 6 species (reflecting six ^{13}C-atoms in the same molecule) which can be explained by the direct incorporation of the supplied [U-$^{13}C_6$]glucose into glycogen or fructose (Fig. 4**B**). The higher fraction of M + 1 to M + 5 in cell wall-derived amino sugars (70–90 %) in comparison to that of glycogen-derived glucose (20 %) could reflect metabolic turnover of glucose phosphate prior to its usage for cell wall synthesis.

Protein-derived amino acids were obtained from acidic hydrolysates of the bacterial pellets. For GC/MS analysis, these amino acids were converted into their TBDMS-derivatives. The measured ^{13}C-incorporation ranked amino acids from Ala > Glu > Ser > Tyr (Fig. 4). The other amino acids were apparently unlabelled probably due to the presence of unlabelled amino acids and peptides in the complex MT composed of brain heart infusion broth, bacto trypton and casamino acids (see also Chen et al., 2017). On the basis of the labelling profiles in amino acids (Fig. 4), some conclusions can be made. [U-$^{13}C_6$]glucose was efficiently

degraded to [U-$^{13}C_3$]pyruvate, which is reflected by the observation of [U-$^{13}C_3$]Ala. However, MS analysis also identified Ala species carrying only one or two ^{13}C-atoms, as reflected by the excess M + 1 and M + 2 mass peaks, respectively. These isotopologs can be explained by the decarboxylation of M + 1 and M + 2 Asp resulting in [$^{13}C_1$]- or [$^{13}C_2$] pyruvate/Ala, respectively. The fractions of these isotopologs even allowed assigning the relative contributions to Ala formation. Similarly as in *Fth*, in F-W12 Ala is mainly (65 %) formed from pyruvate and a minor fraction (35 %) is derived *via* the Asp route. The high fractions of M + 1 and M + 2 and lower fractions of M + 3, M + 4 and M + 5 in Glu indicated high turnover rates between oxaloacetate and α-ketoglutarate in the TCA cycle. The high fractions of [U-$^{13}C_3$]Ser (M + 3) in the fragment containing all three carbon atoms of the original Ser molecule (Ser-390) again showed efficient usage of [U-$^{13}C_6$]glucose present in MT and its conversion into [U-$^{13}C_3$]3-phosphoglycerate *via* glycolysis. The labelling profiles of Tyr were more complicated and contained M + 1 to M + 9 fractions. That could be explained by the formation of erythrose 4-phosphate *via* the PPP and phosphoenolpyruvate (PEP) *via* glycolysis (see below), as degradation products of [U-$^{13}C_6$]glucose in F-W12.

Using methanol as a solvent, more than 20 polar metabolites including free amino acids, TCA intermediates, and free fatty acids were extracted from the dried pellet of the labelled bacteria. The ^{13}C-excess values and isotope distributions in free amino acids were similar to those of protein-derived amino acids indicating metabolic and isotopic *quasi*-steady state when the bacteria were harvested. Free fatty acids and 3-hydroxybutyrate were highly labelled (6–8 %), suggesting that acetyl-CoA is formed through degradation of the labelled glucose at high rates (Fig. 4). Succinate is then formed from acetyl-CoA *via* the TCA cycle. Therefore, it was mainly M + 1 and M + 2 labelled. Lower fractions of M + 3 labelled succinate could indicate fluxes *via* oxaloacetate made by carboxylation of M + 3 pyruvate.

In total, F-W12 utilized glucose as an efficient source for the formation of fructose, glycogen, cell wall, some amino acids, and fatty acids by carbon flux *via* glycolysis (see below), acetyl-CoA formation and its usage for filling up the TCA cycle or serving as a precursor of downstream products (*e.g.* fatty acids).

3.5. Labelling experiments with [1,2-$^{13}C_2$]glucose

In order to confirm that glucose is indeed degraded *via* glycolysis, we performed additional experiments using [1,2-$^{13}C_2$]glucose as a tracer. The usage of [1,2-$^{13}C_2$]glucose either *via* the Entner-Doudoroff pathway or glycolysis can be differed by specific labelling patterns in pyruvate/Ala. Following the Entner-Doudoroff pathway, [1,2-$^{13}C_2$] pyruvate/Ala would result from [1,2-$^{13}C_2$]glucose, whereas [2,3-$^{13}C_2$] pyruvate/Ala would reflect glucose degradation *via* glycolysis. To distinguish between the two scenarios, we have used a thorough analysis of a specific mass fragment at an *m/z* value of 232 (Ala-232) obtained from the GC–MS analysis of silylated Ala. This fragment arises by decarboxylation of the Ala-derivative and therefore reflects a molecular species containing C-2 and C-3 of the original Ala molecule. Mass analysis of this species provided evidence for significant excess of the species at the *m/z* value of 234 similarly to the Ala fragment (Ala-260) containing all three carbon atoms of the original Ala molecule (see also supplemental Fig. S4). On this basis, it can be followed that C-2 and C-3 of Ala carried the ^{13}C-labels. Thus, glucose is degraded *via* glycolysis (EMP pathway) in F-W12 and not *via* the Entner-Doudoroff pathway.

3.6. Labelling experiments with [U-$^{13}C_3$]serine

[U-$^{13}C_3$]serine was taken up by F-W12, which was clearly seen by the ^{13}C-excess in methanol extracted free Ser (4 % ^{13}C-enrichment) and protein-derived Ser (14 %) (Fig. 4). The observed labelling profiles suggested that Ser is degraded to form pyruvate, which is subsequently converted into alanine or acetyl-CoA for *e.g.* fatty acid biosynthesis. However, probably due to the presence of glucose in MT, Ser is not effectively used for gluconeogenesis, as shown by the low incorporation into Phe and Tyr, as well into the sugars (glucose from glycogen, free fructose and amino sugars from cell wall). Overall, the metabolism of Ser in F-W12 is similar to the one in *Fno* (Chen et al., 2017).

3.7. Labelling experiments with [U-$^{13}C_3$]glycerol

With the fraction obtained by methanolic extraction, it was found that glycerol is highly ^{13}C-enriched (93 mol%) from exogenous [U-$^{13}C_3$] glycerol, which suggests efficient uptake of glycerol during the cultivation of F-W12. [U-$^{13}C_3$]glycerol is then metabolized into [U-$^{13}C_3$] pyruvate which formed the detected [U-$^{13}C_3$]-Ala and [U-$^{13}C_3$]lactate species (Fig. 4). *Via* [U-$^{13}C_2$]acetyl-CoA, Asp, Glu, TCA intermediates and free fatty acids mainly acquired the M + 2 signature. Due to the conversion of Asp into pyruvate, Ala and lactate were also found as M + 1 and M + 2 isotopologs (Fig. 4**B**). Tyr was predominantly M + 2 and M + 3 labelled, which indicated the utilization of [U-$^{13}C_3$]glycerol *via* glucogenesis and PPP to form PEP and erythrose 4-phosphate, respectively. Notably, cell wall amino sugars (glucosamine and muramic acid) were highly labelled, which again provides evidence that glycerol serves a good substrate for the formation of glucose phosphate required for cell wall biosynthesis. However, free fructose and glycogen-derived glucose were almost unlabelled, suggesting that unlabelled glucose from the medium can be directly converted into these sugars in F-W12.

3.8. Differential substrate usage

As in our earlier work to analyse the main pathways for the metabolism of glucose, glycerol and Ser by *Francisella* strains grown and labelled in MT (Chen et al., 2017), we now normalized the ^{13}C-enrichments according to the presence of unlabelled glucose, glycerol and Ser in free or polymeric form in MT. On the basis of this normalization, the values from the experiment with [U-$^{13}C_6$]glucose were multiplied by a factor of 8.5, from the experiment with [U-$^{13}C_3$]-Ser by a factor of 1.15, and from the experiment with [U-$^{13}C_3$]glycerol by a factor of 1. The normalized values are shown in Fig. 5. It is obvious that exogenous glucose is most efficiently used for glycogen and cell wall amino sugars. However, significant carbon flux was also detected from glucose *via* glycolysis and downstream processes into Ala, 3-hydroxybutyrate and free fatty acids. The carbon fluxes from Ser and glycerol into the central metabolism were lower (for serine < 5 %, for glycerol < 15 %).

3.9. Analysis of main pathways for the metabolism of glucose and glycerol of Francisella sp. strain W12-1067 ΔMyo mutant strain grown in MT

For further analyses of the core metabolism in F-W12 ΔMyo mutant strain, we performed additional experiments with this mutant growing in MT supplied with 11 mM [U-$^{13}C_6$]glucose or 25 mM [U-$^{13}C_3$]glycerol. Using the same procedures as described above for the F-W12 wild-type strain, we again analysed the isolated sugars from glycogen and cell walls, amino acids derived from proteins and free metabolites. Based on the values for biological replicates and technical replicates, averaged ^{13}C-excess values (mol%) and fractional isotopologue distributions (%) were calculated (Fig. 6).

Experiments with [U-$^{13}C_6$]glucose: As in the wild-type, glucose from glycogen, cell wall-derived amino sugars and free fructose were highly labelled (about 10–12 %, Fig. 6**A**). The major isotopolog of glycogen-derived glucose and free fructose was M + 6 by conversion of [U-$^{13}C_6$] glucose into [U-$^{13}C_n$]glycogen and [U-$^{13}C_6$]fructose. The cell wall-derived amino sugar glucosamine had again higher fractions of M + 1 to M + 5 (about 70 %) than glycogen-derived glucose and free fructose (about 10 %). The ranking of ^{13}C-excess in protein-derived amino acids (Ala > Ser > Glu > Tyr) slightly differed from the order in the wild-type. The isotopolog profiles of amino acids were similar to the ones in the wild-type strain. Because of the highly labelled acetyl-CoA, free

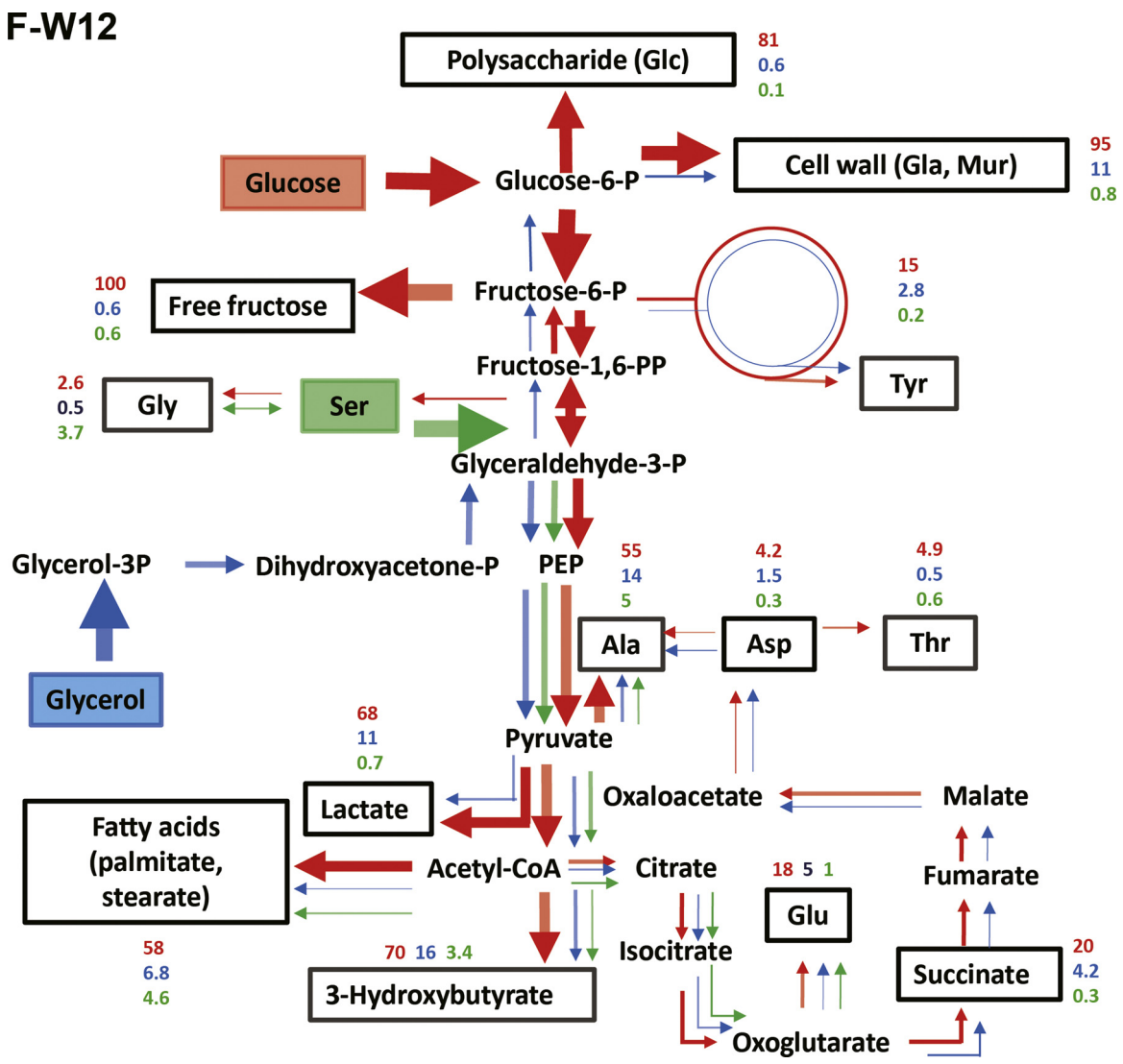

Fig. 5. Metabolic model and observed substrate usages in *Francisella* sp. strain W12-1067 from glucose (red labels), serine (green labels) and glycerol (blue labels). The numbers present the normalized ^{13}C-excess values and the arrow widths indicate the approximate relative fluxes. (For interpretation of the references to colour in this figure legend, the reader is referred to the web version of this article).

fatty acids and 3-hydroxybutyrate acquired the label at rates of 5–7 %. Lactate was also highly labelled (10 %), reflecting its formation from [U-$^{13}C_6$]glucose *via* [U-$^{13}C_3$]pyruvate.

Experiments with [U-$^{13}C_3$]glycerol: Using [U-$^{13}C_3$]glycerol as a precursor, free fructose and glycogen-derived glucose were almost unlabelled (Fig. 6). However, glucosamine was highly labelled (10 %), which could again be explained by gluconeogenetic carbon flux from glycerol into glucose 6-phosphate. [U-$^{13}C_3$]glycerol was also metabolized into [U-$^{13}C_3$]pyruvate, which later formed [U-$^{13}C_3$]-Ala and [U-$^{13}C_3$]lactate. [U-$^{13}C_3$]pyruvate was again degraded to form [U-$^{13}C_2$]acetyl-CoA. Consequently, Glu, TCA intermediates and free fatty acids were mainly M + 2 labelled *via* [U-$^{13}C_2$]acetyl-CoA.

3.10. Differences between the ^{13}C-profiles of Francisella sp. strain W12-1067 and its ΔMyo mutant strain

In Fig. 7**A**, the normalized carbon fluxes for the ΔMyo mutant of F-W12 are shown. The fluxes indicate that glucose was mainly incorporated into glycogen, cell wall amino sugars, alanine and fatty acids. Lower fluxes occurred from glycerol into Ala, lactate and fatty acids. To visualize the differences between the metabolic fluxes of the ΔMyo mutant and its F-W12 wild-type, differences in the normalized ^{13}C-incorporation (ΔMyo mutant – wild-type) are shown by the numbers in Fig. 7**B**. Lower fluxes in the ΔMyo mutant are indicated by negative numeric numbers. It is obvious that the ΔMyo mutant metabolized glucose more efficiently into sugars, Ala and lactate, and less into fatty acids and hydroxybutyrate. Using ^{13}C-glycerol as precursor, higher flux contributions were observed from glycerol into Ala and lactate of the mutant, and less into Tyr and hydroxybutyrate. It can be concluded that, in the mutant, ^{13}C-flux from glucose or glycerol was directed into glycolysis and its downstream products, but less into the PPP due to the absence of enzymes involved in MI metabolism.

4. Discussion

In previous studies, it was shown that amino acids are important for intracellular nutrition (Gesbert et al., 2014, 2015; Ramond et al., 2015; Ziveri et al., 2017), but glycerol and glucose metabolism, as well as gluconeogenesis is important for growth of different *Francisella* species (Brissac et al., 2015; Chen et al., 2017; Radlinski et al., 2018; Ziveri et al., 2017).

Phytate is an important phosphate and carbon storage component of plants and is found at high amounts in fruits, nut seeds, and therefore also in soil and aquatic habitats (Lim et al., 2007). Bacteria, fungi and

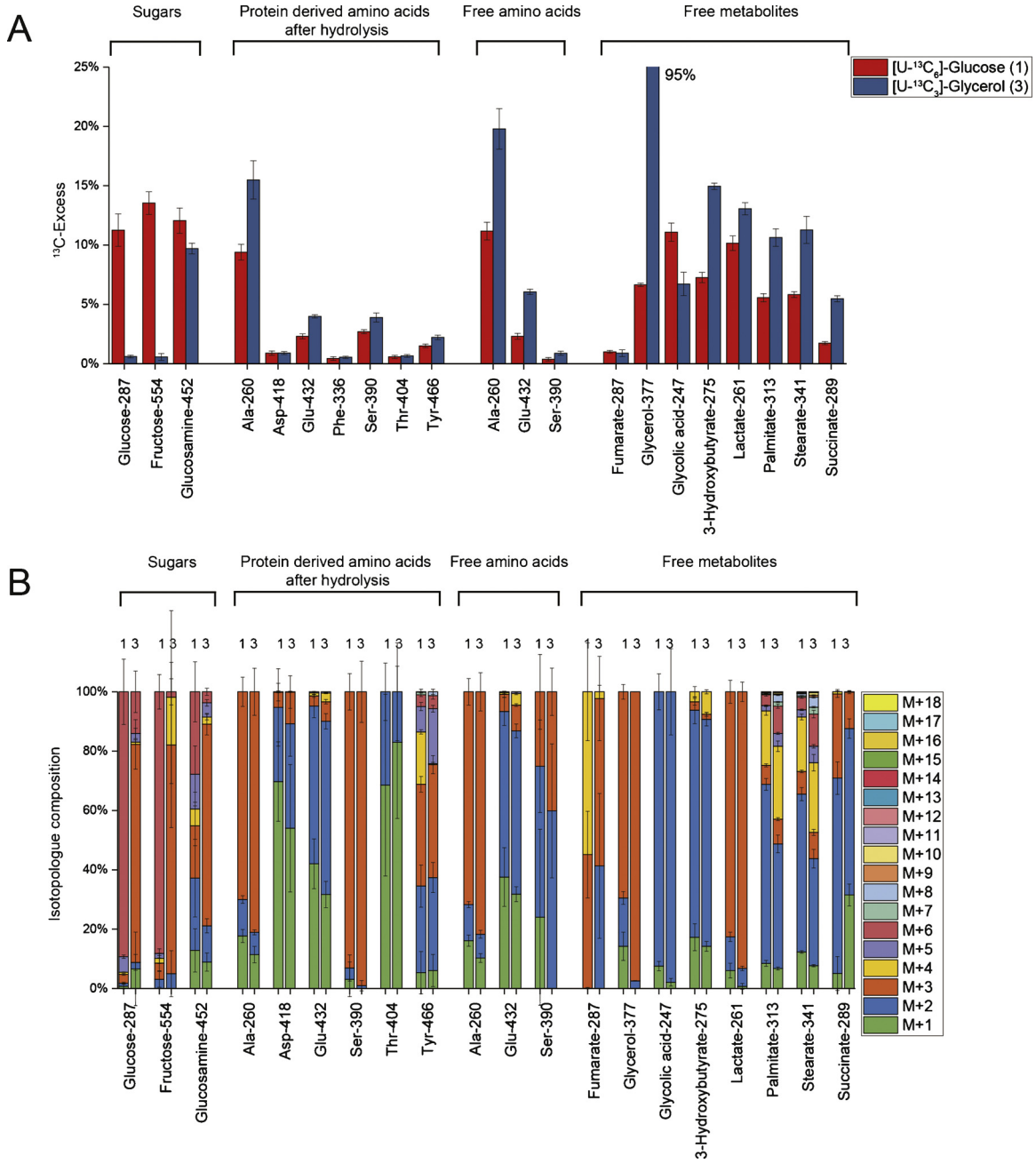

Fig. 6. (A) ^{13}C-Excess (mol%) and **(B)** the fractional isotopolog distributions (%) in key metabolites of the F-W12 ΔMyo mutant grown in MT supplied with 11 mM [U-$^{13}C_6$]glucose (red labels, (1)) or 25 mM [U-$^{13}C_3$]glycerol (blue labels, (3)). ^{13}C-Excess (mol%) and relative fractions of isotopologs (%) were determined by GC/MS of the derivatives of different metabolites at the indexed *m/z* values. Error bars indicate standard deviations from the means of 6 values using 2 × biological replicates and 3 × technical replicates. (For interpretation of the references to colour in this figure legend, the reader is referred to the web version of this article).

plants are able to generate MI from phytate by the enzymatic activity of phytases (MI hexakisphosphate phosphohydrolase) (Rao et al., 2009). We recently identified a new *Francisella* species (water-associated environmental isolate F-W12; (Rydzewski et al., 2014)) and, in this study, *in silico* genome analysis revealed the presence of a putative MI (glucuronate) metabolism pathway in this species. The characteristic MI oxygenase of F-W12 is 81–88 % identical to the respective enzymes of different *Francisella* species and 41 % identical to the respective oxygenase of the plant *Arabidopsis lyrata*. A similar pathway has been previously identified by genome analysis in *Fno* and *F. philomiragia* ATCC 25015, but no experiments were performed to investigate the function of this pathway (Siddaramappa et al., 2011). The pathway was found in isolates with association to aquatic habitats but not in *Ftt* or *Fth* and it was therefore postulated that it represents a more ancient operon that was lost during adaptation to the host organisms (Siddaramappa et al., 2011).

In this study, we could now demonstrate that the main glucuronate-utilization pathway is present in F-W12. Growth and ^{2}H-labelling experiments clearly showed that this pathway is functional in F-W12 for the usage of MI. More specifically, MI supported growth of F-W12 and *Fno* Fx1 in MT-Glc. Final evidence was provided by labelling experiments in CDM-Glc containing MI-C-$^{2}H_6$ as a substrate. Whereas the wild-type strain showed high incorporation of ^{2}H-labelled MI, only minor fluxes from ^{2}H-MI were detected for the mutant strain. Although the MI transport protein (peg 283) was deleted in the mutant strain, small amounts of MI may enter the cell due to the presence of a putative

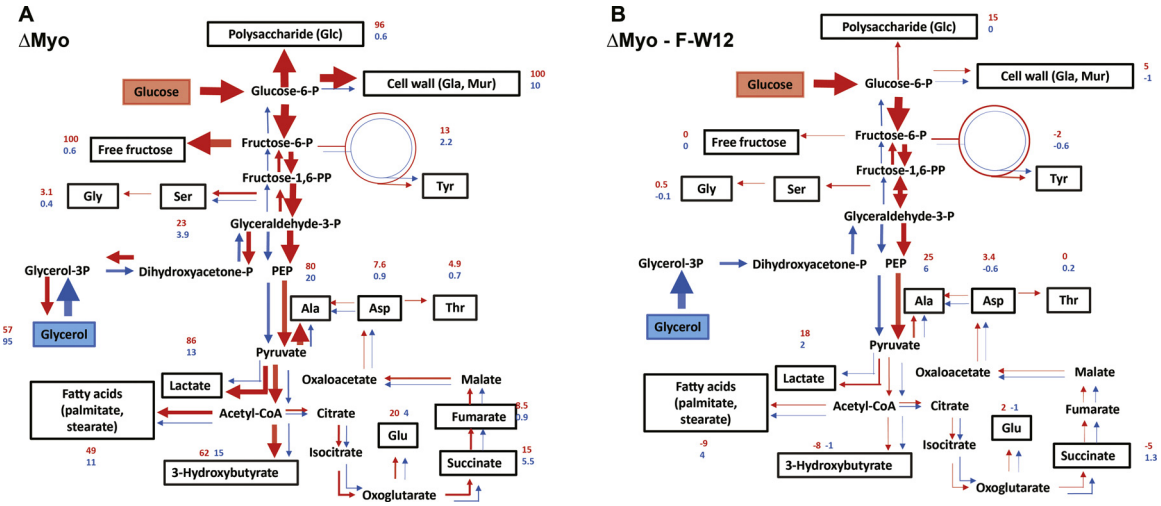

Fig. 7. (A) Observed metabolic pathways and fluxes in F-W12 ΔMyo mutant from exogenous glucose (red labels) and glycerol (blue labels). For more details, see legend to Fig. 5. **(B)** Differences in the metabolic fluxes between F-W12 wild-type and its isogenic ΔMyo mutant. For this, differences in the normalized ^{13}C-incorporation were calculated (values in the experiment with theΔMyo mutant minus the respective values observed for the wild-type). Metabolites detected by GC–MS-analysis are indicated by the black boxes. The numbers indicate normalized overall ^{13}C-incorporation (from labelled glucose and glycerol in red and blue, respectively). The arrow widths roughly indicate the relative fluxes. Fluxes conducive to enrichments < 1 % are not shown. In **(B)** the numbers indicate the differences in the normalized overall ^{13}C-enrichments (ΔMyo mutant – wild-type). Lower fluxes in ΔMyo mutant are indicated by a negative numeric value. (For interpretation of the references to colour in this figure legend, the reader is referred to the web version of this article).

minor MI transporter (peg 112, Pfam MFS_1) or the putative sugar permease (peg 717, Pfam MFS_1). The ^{2}H-incorporation observed in multiple metabolic products leave no doubt that MI-C-$^{2}H_6$ served as an efficient carbon substrate in F-W12. Interestingly, the labelling profile in glucose is explained by its synthesis from M + 1 labelled pyruvate and M + 2 labelled glyceraldehyde-3-P generated by the Eda enzyme (peg 281) known from the Entner-Doudoroff pathway and also present in the MI-utilizing operon of F-W12 (see also supplementary Fig. S2). These precursors are both derived from M + 2 labelled 2-dehydro-3-deoxy-D-gluconate, where the synthesis of pyruvate leads to loss of one deuterium atom resulting in the M + 1 labelling, whereas during the formation of glyceraldehyde-3-P both deuterium atoms are retained leading to the M + 2 labelling. Either precursor enters glycolysis/gluconeogenesis then leading to the observed M + 1 and M + 2 isotopologs in glucose.

To get more clues about the metabolic capacity of the new *Francisella* species, we further investigated the usages of main substrates (glucose, serine and glycerol). Genes involved in the main metabolic pathways of F-W12 are given in supplemental Fig. S3. On this basis, F-W12 has the capacity to metabolize glucose, Ser and glycerol into sugars, protein-derived amino acids, free amino acids and free metabolites, respectively. ^{13}C-Labelling experiments shown in this study demonstrate that glucose serves an efficient precursor to form glycogen and cell wall amino sugars, but can also be degraded *via* EMP not *via* the ED or PPP, to provide the building blocks for amino acids, as well as for fatty acids. However, the usage of glycerol was less active, and lead to incorporation mostly into amino acids (Ala), lactate and fatty acids when strain F-W12 was grown in the presence of additional unlabelled glucose (MT). Exogenous Ser was mainly used directly for protein biosynthesis or for biosynthesis (Ala > Gly > FA > Glu), but was not effectively used for gluconeogenesis.

These data support that F-W12 utilized multiple carbon nutrients following the concepts of a bipartite metabolism (Eisenreich et al., 2015, 2019; Grubmüller et al., 2014). Compared to previous findings using *Fth* and *Fno* (Chen et al., 2017), the whole metabolism of F-W12 seems to be more related to the one of *Fno*, especially for the usage of glycerol and glucose as carbon substrates. The usage of Ser as a carbon source for the generation of Ala is also more similar to *Fno*, whereas fluxes into Gly, lactate and fatty acids are more similar to the earlier findings with *Fth* (Chen et al., 2017).

The ΔMyo mutant of F-W12 lacking the whole MI-utilizing pathway, had a more active EMP and less active PPP, as indicated by the higher ^{13}C-incorporation into Ala, lactate and sugars. Interestingly, when grown in MT, the metabolism of glucose and glycerol in the mutant strain lead to higher incorporation into Ala (Pyr) and lower incorporation into Tyr, indicating that the Eda enzyme in the wild-type strain may not only be involved in the metabolism of MI. The absence of Eda may lead to a higher concentration of pyruvate and glyceraldehyde-3-P, since there is no carbon flux to KDPG (supplementary Fig. S3). The role of the Eda enzyme of the MI gene cluster on glucose metabolism should therefore be further analysed by generating and characterizing a specific ΔEda mutant strain of F-W12.

In conclusion, MI serves as an additional carbon source for F-W12, thus confirming the *in silico* genome data. The labelling data of the F-W12 ΔMyo mutant strain indicated that the Eda enzyme in the wild-type strain may not only be involved in the metabolism of MI or phytate. Moreover, our data are also in agreement with multiple substrate usage by F-W12 using exogenous glucose, Ser and glycerol. The bipartite metabolism of F-W12 could be an argument for host specific virulence or persistence within the environment. For *L. pneumophila*, an aquatic human pathogen replicating in amoeba and other protozoa in its environmental habitat, it has been demonstrated that MI is supporting the multiplication of *L. pneumophila* in macrophages and amoebae (Manske et al., 2016). *L. pneumophila* also exhibits a bipartite metabolism (Eisenreich and Heuner, 2016; Gillmaier et al., 2016; Häuslein et al., 2016, 2017). In addition, phytate has a role for intracellular growth restriction of *L. pneumophila* in amoebae and the phytase of *L. pneumophila* counteracts this restriction (Weber et al., 2014)., For *Francisella* further research is needed to investigate the enzymatic activity and the role of the putative phytase in F-W12 to elucidate if phytate can be used and may be causative for the persistence of *Francisella* species at least within the aquatic habitat.

Declaration of Competing Interest

All authors declare no conflict of interests.

Acknowledgments

This work received financial support from the Deutsche Forschungsgemeinschaft (EI 384/11) and the Robert Koch Institute. We thank Thomas Geisberger and Claudia Huber for help. The funders had no role in study design, data collection and analysis, decision to publish or preparation of the manuscript. No financial conflicts of interest regarding the contents of the manuscript and its authors exist.

Appendix A. Supplementary data

Supplementary material related to this article can be found, in the online version, at doi:https://doi.org/10.1016/j.ijmm.2020.151426.

References

Ahmed, Z., Zeeshan, S., Huber, C., Hensel, M., Schomburg, D., Munch, R., Eylert, E., Eisenreich, W., Dandekar, T., 2014. 'Isotopo' a database application for facile analysis and management of mass isotopomer data. Database (Oxford) 2014.

Anderson, W.A., Magasanik, B., 1971. The pathway of myo-inositol degradation in *Aerobacter aerogenes*. Conversion of 2-deoxy-5-keto-D-gluconic acid to glycolytic intermediates. J. Biol. Chem. 246, 5662–5675.

Ashwell, G., Wahba, A.J., Hickman, J., 1960. Uronic acid metabolism in bacteria. I. Purification and properties of uronic acid isomerase in *Escherichia coli*. J. Biol. Chem. 235, 1559–1565.

Becker, S., Lochau, P., Jacob, D., Heuner, K., Grunow, R., 2016. Successful re-evaluation of broth medium T for the growth of *Francisella tularensis* ssp. and other higly pathogenic bacteria. J. Microbiol. Meth. 121, 5–7.

Bertani, G., 1951. Studies on lysogenesis. I. The mode of phage liberation by lysogenic *Escherichia coli*. J. Bacteriol. 62, 293–300.

Bertani, G., 2004. Lysogeny at mid-twentieth century: P1, P2, and other experimental systems. J. Bacteriol. 186, 595–600.

Brissac, T., Ziveri, J., Ramond, E., Tros, F., Kock, S., Dupuis, M., Brillet, M., Barel, M., Peyriga, L., Cahoreau, E., Charbit, A., 2015. Gluconeogenesis, an essential metabolic pathway for pathogenic *Francisella*. Mol. Microbiol. 98, 518–534.

Challacombe, J.F., Petersen, J.M., Gallegos-Graves, V., Hodge, D., Pillai, S., Kuske, C.R., 2017. Whole-genome relationships among *Francisella* bacteria of diverse origins define new species and provide specific regions for detection. Appl. Environ. Microbiol. 83.

Chamberlain, R.E., 1965. Evaluation of live tularemia vaccine prepared in a chemically defined medium. Appl. Microbiol. 13, 232–235.

Chen, F., Rydzewski, K., Kutzner, E., Häuslein, I., Schunder, E., Wang, X., Meighen-Berger, K., Grunow, R., Eisenreich, W., Heuner, K., 2017. Differential substrate usage and metabolic fluxes in *Francisella tularensis* subspecies holarctica and *Francisella novicida*. Front. Cell. Infect. Microbiol. 7, 275.

Clarridge 3rd, J.E., Raich, T.J., Sjosted, A., Sandstrom, G., Darouiche, R.O., Shawar, R.M., Georghiou, P.R., Osting, C., Vo, L., 1996. Characterization of two unusual clinically significant *Francisella* strains. J. Clin. Microbiol. 34, 1995–2000.

Eisenreich, W., Heuner, K., 2016. The life stage-specific pathometabolism of *Legionella pneumophila*. FEBS Lett. 590, 3868–3886.

Eisenreich, W., Dandekar, T., Heesemann, J., Goebel, W., 2010. Carbon metabolism of intracellular bacterial pathogens and possible links to virulence. Nat. Rev. Microbiol. 8, 401–412.

Eisenreich, W., Heesemann, J., Rudel, T., Goebel, W., 2015. Metabolic adaptations of intracellullar bacterial pathogens and their mammalian host cells during infection ("Pathometabolism"). Microbiol. Spectr. 3.

Eisenreich, W., Rudel, T., Heesemann, J., Goebel, W., 2019. How viral and intracellular bacterial pathogens reprogram the metabolism of host cells to allow their intracellular Replication. Front. Cell.Infect. Microbiol. 9, 42.

Ellis, J., Oyston, P.C., Green, M., Titball, R.W., 2002. Tularemia. Clin. Microbiol. Rev. 15, 631–646.

Eylert, E., Schar, J., Mertins, S., Stoll, R., Bacher, A., Goebel, W., Eisenreich, W., 2008. Carbon metabolism of *Listeria monocytogenes* growing inside macrophages. Mol. Microbiol. 69, 1008–1017.

Faber, M., Heuner, K., Jacob, D., Grunow, R., 2018. Tularemia in Germany-A re-emerging zoonosis. Front. Cell. Infect. Microbiol. 8, 40.

Gesbert, G., Ramond, E., Rigard, M., Frapy, E., Dupuis, M., Dubail, I., Barel, M., Henry, T., Meibom, K., Charbit, A., 2014. Asparagine assimilation is critical for intracellular replication and dissemination of *Francisella*. Cell. Microbiol. 16, 434–449.

Gesbert, G., Ramond, E., Tros, F., Dairou, J., Frapy, E., Barel, M., Charbit, A., 2015. Importance of branched-chain amino acid utilization in *Francisella* intracellular adaptation. Infect. Immun. 83, 173–183.

Gillmaier, N., Schunder, E., Kutzner, E., Tlapak, H., Rydzewski, K., Herrmann, V., Stammler, M., Lasch, P., Eisenreich, W., Heuner, K., 2016. Growth-related metabolism of the carbon storage poly-3-hydroxybutyrate in *Legionella pneumophila*. J. Biol. Chem. 291, 6471–6482.

Grubmüller, S., Schauer, K., Goebel, W., Fuchs, T.M., Eisenreich, W., 2014. Analysis of carbon substrates used by *Listeria monocytogenes* during growth in J774A.1 macrophages suggests a bipartite intracellular metabolism. Front. Cell. Infect. Microbiol. 4, 156.

Gyuranecz, M., Erdelyi, K., Fodor, L., Janosi, K., Szepe, B., Fuleki, M., Szoke, I., Denes, B., Makrai, L., 2010. Characterization of *Francisella tularensis* strains, comparing their carbon source utilization. Zoon. Public Health 57, 417–422.

Häuslein, I., Manske, C., Goebel, W., Eisenreich, W., Hilbi, H., 2016. Pathway analysis using (13) C-glycerol and other carbon tracers reveals a bipartite metabolism of *Legionella pneumophila*. Mol. Microbiol. 100, 229–246.

Häuslein, I., Sahr, T., Escoll, P., Klausner, N., Eisenreich, W., Buchrieser, C., 2017. *Legionella pneumophila* CsrA regulates a metabolic switch from amino acid to glycerolipid metabolism. Open Biol. 7 pii: 170149.

Huber, B., Escudero, R., Busse, H.J., Seibold, E., Scholz, H.C., Anda, P., Kampfer, P., Splettstoesser, W.D., 2010. Description of *Francisella hispaniensis* sp. nov., isolated from human blood, reclassification of *Francisella novicida* (Larson et al. 1955) Olsufiev et al. 1959 as *Francisella tularensis* subsp. *novicida* comb. nov. and emended description of the genus *Francisella*. Int. J. Syst. Evol. Microbiol. 60, 1887–1896.

Kilgore, W.W., Starr, M.P., 1959. Catabolism of galacturonic and glucuronic acids by *Erwinia carotovora*. J. Biol. Chem. 234, 2227–2235.

Köppen, K., Chen, F., Rydzewski, K., Einenkel, R., Böttcher, T., Morguet, C., Grunow, R., Eisenreich, W., Heuner, K., 2019. Screen for fitness and virulence factors of *Francisella* sp. strain W12-1067 using amoebae. Int. J. Med. Microbiol. 309, 151341.

Kröger, C., Stolz, J., Fuchs, T.M., 2010. Myo-Inositol transport by *Salmonella enterica* serovar Typhimurium. Microbiol. 156, 128–138.

Larson, C.L., Wicht, W., Jellison, W.L., 1955. A new organism resembling *P. Tularensis* isolated from water. Public Health Rep. 70, 253–258.

Lee, W.N., Byerley, L.O., Bergner, E.A., Edmond, J., 1991. Mass isotopomer analysis: theoretical and practical considerations. Biol. Mass Spectrom. 20, 451–458.

Lim, B.L., Yeung, P., Cheng, C., Hill, J.E., 2007. Distribution and diversity of phytate-mineralizing bacteria. Int. Soc. Microb. Ecol. J. 1, 321–330.

Manske, C., Schell, U., Hilbi, H., 2016. Metabolism of myo-inositol by *Legionella pneumophila* promotes infection of amoebae and macrophages. Appl. Environ. Microbiol. 82, 5000–5014.

Meibom, K.L., Charbit, A., 2010. *Francisella tularensis* metabolism and its relation to virulence. Front. Microbiol. 1, 140.

O'Shaughnessy, J.B., Chan, M., Clark, K., Ivanetich, K.M., 2003. Primer design for automated DNA sequencing in a core facility. Biotechniques 35 (112–116), 118–121.

Pavlovich, N.V., Mishan'kin, B.N., 1987. Transparent nutrient medium for culturing *Francisella* tularensis. Antibiot. Med. Biotekhnol. 32, 133–137.

Peekhaus, N., Conway, T., 1998. What's for dinner?: entner-Doudoroff metabolism in *Escherichia coli*. J. Bacteriol. 180, 3495–3502.

Qu, P.H., Li, Y., Salam, N., Chen, S.Y., Liu, L., Gu, Q., Fang, B.Z., Xiao, M., Li, M., Chen, C., Li, W.J., 2016. *Allofrancisella inopinata* gen. nov., sp. nov. and *Allofrancisella frigidaquae* sp. nov., isolated from water-cooling systems, and transfer of *Francisella guangzhouensis* Qu et al. 2013 to the new genus as *Allofrancisella guangzhouensis* comb. nov. Int. J. Syst. Evol. Microbiol. 66, 4832–4838.

Radlinski, L.C., Brunton, J., Steele, S., Taft-Benz, S., Kawula, T.H., 2018. Defining the metabolic pathways and host-derived carbon substrates required for *Francisella tularensis* intracellular growth. MBio 9.

Ramond, E., Gesbert, G., Rigard, M., Dairou, J., Dupuis, M., Dubail, I., Meibom, K., Henry, T., Barel, M., Charbit, A., 2014. Glutamate utilization couples oxidative stress defense and the tricarboxylic acid cycle in *Francisella* phagosomal escape. PLoS Pathog. 10, e1003893.

Ramond, E., Gesbert, G., Guerrera, I.C., Chhuon, C., Dupuis, M., Rigard, M., Henry, T., Barel, M., Charbit, A., 2015. Importance of host cell arginine uptake in *Francisella* phagosomal escape and ribosomal protein amounts. Mol. Cell Proteomics 14, 870–881.

Rao, D.E., Rao, K.V., Reddy, T.P., Reddy, V.D., 2009. Molecular characterization, physicochemical properties, known and potential applications of phytases: an overview. Crit. Rev. Biotechnol. 29, 182–198.

Rydzewski, K., Schulz, T., Brzuszkiewicz, E., Holland, G., Luck, C., Fleischer, J., Grunow, R., Heuner, K., 2014. Genome sequence and phenotypic analysis of a first German *Francisella* sp. isolate (W12-1067) not belonging to the species *Francisella tularensis*. BMC Microbiol. 14, 169.

Siddaramappa, S., Challacombe, J.F., Petersen, J.M., Pillai, S., Hogg, G., Kuske, C.R., 2011. Common ancestry and novel genetic traits of *Francisella novicida*-like isolates from North America and Australia as revealed by comparative genomic analyses. Appl. Environ. Microbiol. 77, 5110–5122.

Sjostedt, A., 2011. Special Topic on *Francisella tularensis* and Tularemia. Front. Microbiol. 2, 86.

Tlapak, H., Koppen, K., Rydzewski, K., Grunow, R., Heuner, K., 2018. Construction of a new phage integration vector pFIV-Val for use in different *Francisella* species. Front. Cell. Infect. Microbiol. 8, 75.

Turner, B.L., Paphazy, M.J., Haygarth, P.M., McKelvie, I.D., 2002. Inositol phosphates in the environment. Philos. Trans. R. Soc. Lond., B, Biol. Sci. 357, 449–469.

Vallesi, A., Sjodin, A., Petrelli, D., Luporini, P., Taddei, A.R., Thelaus, J., Ohrman, C., Nilsson, E., Di Giuseppe, G., Gutierrez, G., Villalobo, E., 2018. A New Species of the gamma-Proteobacterium *Francisella, F. adeliensis* Sp. Nov., endocytobiont in an antarctic marine ciliate and potential evolutionary forerunner of pathogenic species. Microb. Ecol.

Weber, S., Stirnimann, C.U., Wieser, M., Frey, D., Meier, R., Engelhardt, S., Li, X., Capitani, G., Kammerer, R.A., Hilbi, H., 2014. A type IV translocated *Legionella* cysteine phytase counteracts intracellular growth restriction by phytate. J. Biol. Chem. 289, 34175–34188.

Yoshida, K., Yamaguchi, M., Morinaga, T., Kinehara, M., Ikeuchi, M., Ashida, H., Fujita, Y., 2008. Myo-Inositol catabolism in *Bacillus subtilis*. J. Biol. Chem. 283, 10415–10424.

Ziveri, J., Barel, M., Charbit, A., 2017. Importance of metabolic adaptations in *Francisella* pathogenesis. Front. Cell. Infect. Microbiol. 7, 96.